minerals

MDPI

Article

The Role of Reduced Surface Sulfur Species in the Removal of Se(VI) by Sulfidized Nano Zero-Valent Iron

Stefan Peiffer [1,*], John Mohanraj [2], Kerstin Hockmann [1,3], Jörg Göttlicher [4], Mukundan Thelakkat [2,5] and Bouchra Marouane [1]

[1] Department of Hydrology, BayCEER, University of Bayreuth, 95440 Bayreuth, Germany; kerstin.hockmann@geochem.uni-freiburg.de (K.H.); bouchra.marouane@upm.com (B.M.)
[2] Applied Functional Polymers, University of Bayreuth, 95440 Bayreuth, Germany; mail.johnmohanraj@gmail.com (J.M.); mukundan.thelakkat@uni-bayreuth.de (M.T.)
[3] Applied Geochemistry, University of Freiburg, 79104 Freiburg, Germany
[4] Institute for Photon Science and Synchrotron Radiation, Karlsruhe Institute of Technology, 76344 Eggenstein-Leopoldshafen, Germany; joerg.goettlicher@kit.edu
[5] Bavarian Polymer Institute, University of Bayreuth, 95440 Bayreuth, Germany
* Correspondence: s.peiffer@uni-bayreuth.de

Abstract

Sulfidized nano zero-valent iron (S-nZVI) particles are known to stimulate the reductive removal of various oxyanions due to enhanced electron selectivity and electron conductivity between the Fe(0) core and the target compound. Sulfidation creates a number of reactive sulfur species, the role of which has not yet been investigated in the context of S-nZVI. In this study, we investigated the contribution of reactive sulfur species to Se(VI) reduction by S-nZVI at different molar S/Fe ratios (0, 0.1 and 0.6) and Se(VI) concentrations (0, 5 and 50 mg L^{-1}). In the presence of S-nZVI, the rate of reduction was accelerated by a factor of up to ten. X-ray Absorption Near-Edge Structure (XANES) spectroscopy and surface-sensitive X-ray photoelectron spectroscopy (XPS) identified Se(0) as the predominant reduction product (~90%). The reduction reaction was accompanied by a loss of FeS and the formation of surface-bound Fe(II) polysulfide (FeSx) and S(0) species. Likewise, wet chemical extraction techniques suggested a direct involvement of acid volatile sulfide (AVS) species (surface-bound FeS) in the reduction of Se(IV) to Se(0) and formation of S(0). Mass balance estimates reveal that between 9 and 15% of the conversion of Se(0) originates from oxidation of FeS to FeSx. From these findings, we propose that surface-bound Fe sulfide species are important but previously overlooked reactants contributing to the reduction of oxyanions associated with S-nZVI particles, as well as in natural environments undergoing sulfidation reactions.

Keywords: sulfidation; nano zero-valent iron; surface bound sulfur species; reduction; selenium(VI)

Academic Editor: Jianxi Zhu

Received: 9 December 2025
Revised: 2 January 2026
Accepted: 5 January 2026
Published: 9 January 2026

1. Introduction

Reductive removal of contaminants by ZVI in the presence of dissolved oxygen is considered the result of oxidation of Fe(0) by O_2 and subsequent formation of highly reactive Fe(II) containing solid intermediates, such as $Fe(OH)_2$ and Fe_3O_4 [1,2]. Application of ZVI under field conditions, i.e., in the presence of oxygen and groundwater, is regarded to be limited since a large fraction of electrons potentially available for contaminant reduction by ZVI is channelled into corrosion reactions and therefore, the capacity of ZVI for reduction of the target compound is decreased [2].

In order to overcome such limitations in the application of ZVI, sulfidation of nanoparticles of ZVI has received growing attention in the last decade [3,4]. Enhancement of reactivity upon sulfidation of nZVI was attributed to an increase in the specific surface area of nZVI and in adsorption capacity, as well as to the facilitation of electron transfer from the Fe(0) core to the adsorbed contaminant by the sulfidized layer [5]. In particular, the formation of a shell consisting of reduced iron sulfur species is regarded to enhance the electron efficiency of ZVI towards targeted contaminants under aerobic conditions [2,5]. Hence, the sulfidation of ZVI was found to prevent the passivation of ZVI by a reaction with dissolved oxygen and also enhance the specificity of the reaction with a target contaminant [5,6]. Sulfidation of ZVI also increased the reductive removal of Se(VI) by a factor of 10 relative to pure ZVI, with Se(0) being a major reaction product [7]. In their study, the authors attributed the role of sulfidation to the acceleration of aerobic Fe(0) corrosion, which in turn facilitated Se(VI) removal [7].

In contrast, direct involvement of reduced sulfur species during ZVI sulfidation has been proposed to enhance Cr(VI) reduction [5,6,8]. The formation of an FeS layer prevents particle aggregation and subsequently increases the BET surface area and stimulates the formation of highly reactive sites at the FeS coating, facilitating electron transfer.

Similarly, sulfidation of ferric (oxy) hydroxides and subsequent formation of highly reactive sulfur species has stimulated the reduction of oxyanions such as Sb(V), Cr(VI), and U(VI) [9,10]. Yet, systematic studies about the reactivity of sulfidized ferric oxide surface species towards oxoanions do not exist; however, involvement of these species in the reduction of Sb(V) to Sb(III) may be indirectly inferred from observations made during sulfide-induced iron oxide transformations in the presence of Sb(V) [7]. Mackinawite may be a good surrogate for surface-bound FeS, with clear evidence of its ability to reduce As(V) to As(III) or lower valences [11]. Similarly, Cr(V) was effectively reduced by pure mackinawite (FeS) [12,13] with clear indications for the involvement of surface-bound amorphous FeS [8,13]. There is some indication that Se(VI) could be reduced to Se(0) [14].

In this study, we aim to disentangle the contribution of reduced sulfur species to electron transfer from sulfidized nano ZVI particles (S-nZVI) to selenate (Se(VI), SeO_4^{2-}). Selenate is well known to cause severe contamination of natural waters and aquatic environments due to its toxicity, bioavailability and mobility [15]. It may be highly enriched in soils and cause severe health problems in affected populations [16]. Hence, removal of these anions has fueled a large number of research activities [17,18]. Among the methods used, application of zero-valent iron (ZVI) turned out to be a promising approach to sequester selenate by chemical reduction to immobile species [1,19]. Here, we reacted S-nZVI particles produced at a high and low S/Fe ratio (0.6 and 0.1, respectively) with different concentrations of Se(VI). The S/Fe ratio is regarded to be a key parameter to control the reactivity and removal capacity of S-ZVI for various contaminants [3]. We studied surface-bound sulfur species by X-ray photoelectron spectroscopy (XPS), complemented by mass balance analysis of reduced sulfur species through wet-chemistry techniques.

2. Materials and Methods

2.1. Material and Chemical Reagents

Iron nanoparticles (n-ZVI) were purchased as NANOFER STAR from a commercial supplier (NANO IRON s.r.o., Židlochovicem, Czech Republic). The nZVI material was covered by a thin layer of iron oxides (~18 wt. % Fe_3O_4 and ~8 wt. % FeO; for information from the supplier, cf. Supporting Information). The nZVI materials were sulfidized with Na_2S in an activation process to obtain molar S/Fe ratios of 0.1 and 0.6, respectively (cf. Table S1).

The sulfidation procedure followed a method described in detail in the Supporting Information (cf. Figures S1–S3 in the Supplementary Material) [20]. All reagents used in these experiments were of analytical grade and used without further purification (Na_2S, Na_2SeO_4, Na_2SeO_3 and Se(0) from Sigma Aldrich, Taufkirchen, Germany, >98% and ZnSe from Thermo Fischer Scientific, Darmstadt, Germany, >99%).

2.2. Batch Experiments

All experiments were performed in duplicates under gentle stirring at room temperature under ambient atmospheric conditions. Se(VI) concentration was added as Na_2SeO_4 (0, 5 and 50 mg Se(VI) L^{-1}) to the reaction vessels, each containing either 1 g of nZVI or S-nZVI, suspended in a 1 L NaCl electrolyte solution (c = 0.01 mol L^{-1}). At predetermined time intervals, the pH of the solution was determined, and 10 mL of the sample was removed from the reactor and immediately filtered through a 0.45 µm filter membrane. After 48 h, at the end of the experiments, the solid and aqueous phases were separated by centrifugation. The aqueous phase was filtered through a <0.45 µm filter, acidified with HNO_3 and analyzed for total Se, total Fe and total S using inductively coupled plasma–optic emission spectroscopy (ICP-OES). In addition, the concentration of Fe(II) in the filtrates was determined photometrically by the phenanthroline method [21]. The solid particles were dried and stored inside a glovebox under a nitrogen atmosphere until further analysis.

2.3. Characterization of ZVI Particles

Surface morphology and elementary composition of both nZVI and S-nZVI particles were characterized by scanning electron microscopy (SEM) coupled with energy-dispersive X-ray spectroscopy (EDX). The surface area was determined by the five-point N2 point adsorption isotherm (BET) method (Gemini 2375, Micromeritics Instrument Corporation, Norcross, GA, USA). X-ray diffraction (XRD) was carried out on the ground nZVI and S-nZVI specimens before and after the experiments using Co Kα radiation (D5000, Siemens, München, Germany). Diffractograms were evaluated using the DIFFRAC-plus evaluation software package (Bruker AXS, Karlsruhe, Germany). Cryogenic X-ray photoelectron spectra (XPS) were measured with a PHI 5000 VersaProbe III system (ULVAC-PHI, Inc., Chigasaki, Japan) fitted with an Al Kα excitation source (hν = 1486.6 eV) and a dual neutralizer (electron gun and Ar^+) at 10^{-9} mbar pressure and 140 ± 10 K. For experimental details, cf. SI Methods Section. Selenium K-edge (12,658 eV) X-ray Absorption Near-Edge Structure (XANES) spectra were collected at the SUL-X beamline of the synchrotron radiation source at KIT (Karlsruhe, Germany) to investigate Se speciation in the solid phase. The Athena software (0.8.056 from Iffefit package 1.2.11) was used for background subtraction and edge-height normalization [22].

The solid particles obtained before and after reaction with selenate were analyzed sequentially for their contents of acid volatile sulfur (AVS) and of chromium reducible sulfur (CRS). To this end, the AVS content (comprising amorphous FeS) of the wet sediment was determined after hot acid digestion (c = 0.5 mol L^{-1} HCl) and trapping of the sulfide released in NaOH solution (c = 0.2 mol L^{-1}) [23], which was then measured photometrically by the methylene blue method [24]. Subsequently, the CRS content of the same sample was determined after reduction with $Cr(II)Cl_2$ to H_2S. CRS is generally considered to comprise pyrite (FeS_2) and S(0), including polysulfides [23]. Total S content was determined after digestion with aqua regia and subsequent determination of the S content by ICP-OES.

3. Results and Discussion

3.1. Reaction of S-nZVI in the Absence of Se

The major phase identified in the bare nZVI by XRD prior to reaction with Se(VI) (Figure 1a) was α-Fe(0) with a characteristic diffraction peak at 52.5° 2θ [25]. We attributed the small diffraction peak at approximately 47° 2θ to wustite (FeO), which has been reported to be a characteristic product in ZVI corrosion [20,26,27] although its most intensive reflection reported in the literature is often located at slightly higher angles (49° 2θ, [28]). Sulfidation clearly affected the XRD patterns with the characteristic peak of magnetite (Fe_3O_4) at 42° 2θ being clearly visible at the highest S/Fe ratio (Figure 1a). The 48 h corrosion process increased these signals and generally enhanced the noise of the diffractograms, while the wustite signals became very small or even undetectable (Figure 1c,d).

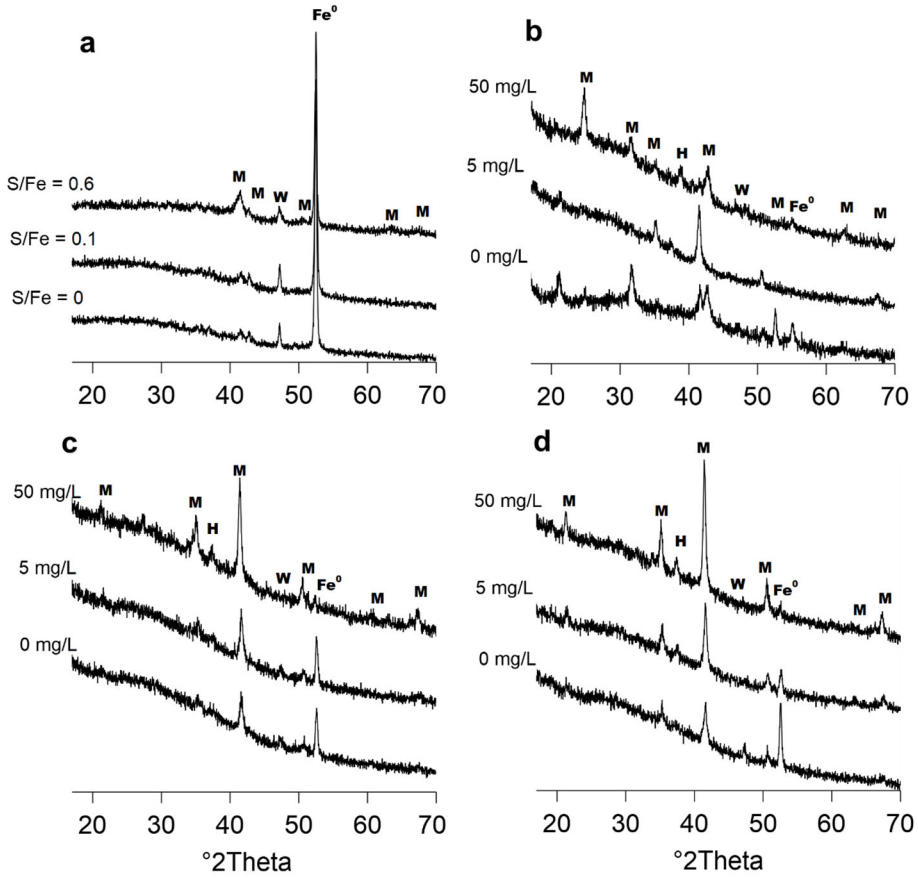

Figure 1. XRD patterns of (**a**) nZVI at different S/Fe ratios before the reaction with Se(IV), (**b**) S-nZVI at a ratio S/Fe = 0, (**c**) S-nZVI at a ratio S/Fe = 0.1 and (**d**) S-nZVI at a ratio S/Fe = 0.6 after reaction with Se(VI) at 0, 5 and 50 mg L^{-1} for 48 h at pH 8. Fe = iron; H = halite; M = magnetite and W = wustite.

In all experiments, the peak intensity of Fe(0) and of wustite in the absence of Se(VI) decreased during the 48 h of the experiment (Figure 1b–d; 0 mg L^{-1}). The decrease in the Fe(0) signal was most pronounced with pure ZVI (Figure 1b; 0 mg L^{-1}), while sulfidation appears to conserve Fe(0) prior to reaction with Se(VI) (Figure 1c,d; 0 mg L^{-1}).

Sulfur-containing phases were not identified with XRD, which is presumably due to the low S contents, material loss during preparation or sampling and/or a low degree of crystallinity [4,20].

The BET specific surface area (SSA) only slightly increased from 20.9 m^2 g^{-1} (determined after nZVI activation) to an average of 27.8 m^2 g^{-1} after sulfidation, which is in accordance with S-nZVI particles produced with the same protocol [27]. SEM images of the

unreacted material display tiny particles with a diameter ranging between 20 and 50 nm that appear to form larger aggregates upon sulfidation (Figure S3). In contrast to bulk XRD measurements, quantitative EDX analysis of the S–nZVI showed distinct peaks of S. The S peak area increased with an increase in the S/Fe ratio (Figure S4), indicating the presence of S upon sulfidation.

The mean S content of the S-nZVI particles was 0.39 and 5.1 wt. % for the S/Fe ratios of 0.1 and 0.6, respectively (Table S1). These values are in a range of S-nZVI particles produced with the same manufacturing recipe [27] but are distinctly lower than values reported for sulfidized ZVI particles produced in the micrometre range [5]. Sulfur could be recovered almost exclusively as AVS with recovery rates of ~100% (Table S1). The recovery of S after 48 h reaction in the absence of Se as total reduced inorganic sulfur (TRIS) by use of the combined AVS and CRS extraction was 87% for the high S/Fe ratio and 63% for the low ratio (Table 1), indicating losses of the added sulfide either by oxidation of sulfur species with an oxidation state > 0, particularly at the low S/Fe ratio, or by degassing of H_2S. The fraction of total dissolved S after 48 h of reaction was low, with 2.3% at the low S/Fe ratio (0.1 mg S g^{-1}) and 7% (3.4 mg S g^{-1}) at the S/Fe ratio of 0.6. Collectively, our data imply that exposure of S-nZVI to water for 48 h led to the formation of S recoverable as CRS, accompanied by some loss of S, presumably by degassing of H_2S.

Table 1. Acid volatile sulfur (AVS) and chromium reducible sulfur (CRS) contents of S-nZVI after 48 h reaction time, errors refer to standard deviation from duplicate measurements. Se(VI) concentrations were converted to molar selenate concentrations and normalized to the particle content (1 g L^{-1}). Total reduced inorganic sulfur (TRIS) was calculated as the sum of AVS and CRS. Total S contents were 3.9 and 51.3 mg g^{-1} for S/Fe ratios of 0.1 and 0.6 (Table S1).

S/Fe Ratio	Reaction Time [h]	SeO_4^{2-} Added [µmol g^{-1}]	AVS [µmol g^{-1}]		CRS [µmol g^{-1}]		TRIS [µmol g^{-1}]	Recovery of Total S as TRIS [%]
			Mean	Std. Dev. (n = 2)	Mean	Std. Dev. (n = 2)		
0	0	0	7.8	0.11	0.72	0.11		
	48	0	0.0	-	0.0	-	0.1	
		63	0.0	-	3.4	-	3.4	
		630	0.0	-	6.9	0.8	6.9	
0.1	0		181.9	3.8	2.4	0.65	184.3	156
	48	0	39.4	24.5	45.9	15.8	85.3	63
		63	20.5	1.1	43.4	22.0	63.9	
		630	3.6	-	81.2	5.1	84.8	
0.6	0		2120.0	102.4	11.2	1.1	2131.2	109
	48	0	458.0	157.5	864.3	321	1322.3	87
		63	116.7	-	1003.9	153	1120.7	
		630	115.6	-	1132.5	-	1248.1	

The influence of the sulfidation process on the oxidation state of Fe and S at the surface of nZVI, and the concentration of surface-bound S species, was probed via X-ray photoelectron spectroscopy (XPS). The detailed spectra of S-nZVI particles with S/Fe = 0, 0.1 and 0.6 measured at Fe2p3/2 and S2p regions are displayed in Figure 2. The Fe2p spectra of all the samples show a peak maximum at ca. 711 eV without any trace of a peak/shoulder in the lower binding energy region, indicating the absence of Fe(0) on the surface. The Fe2p spectrum of S-free nZVI particles after nZVI activation was refined based on a model described by Gupta & Sen [29] and applied by Biesinger et al. [30]. This analysis results in four peaks with a first maximum at 710.3 eV, suggesting the presence of only Fe(III) species on the surface (Figure 2a, top). This is in line with the observation of Li et al. [31], in which the presence of Fe(III) as oxides and oxyhydroxides on the nZVI surface is reported.

Given the low intensity of the peaks compared to sulfidized nZVI samples, the thickness of the surface-bound Fe(III) components formed in the absence of S appears to be thin, as reported for the activation of the particles in use [26].

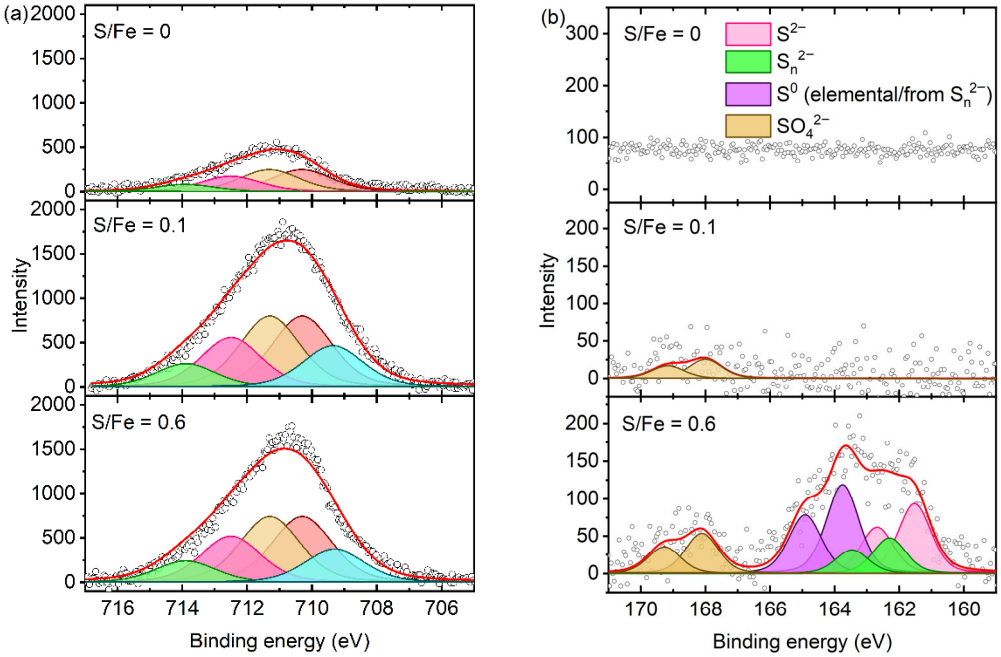

Figure 2. Detailed elemental analysis using XPS signals of S-nZVI in the absence of Se(VI) with S/Fe = 0, 0.1 and 0.6 measured at (**a**) Fe2p3/2 and (**b**) S2p regions with peak fits.

For S-nZVI particles with S/Fe = 0.1 and 0.6, satisfactory fitting of their Fe2p spectra required an additional peak at 709.3 eV along with Fe(III) peaks. Notably, given the complexity of fitting the Fe2p region with multiple Fe components, here this peak was arbitrarily added only to highlight the change in the chemical state of surface Fe due to the sulfidation process. Complementarily, the observed S2p signals from S-nZVI particles with S/Fe = 0.1 and 0.6 evidence the presence of Fe-S-based compounds on the surface of the particles. Peak fitting of the S2p spectrum of S-nZVI with S/Fe = 0.6 reveals the presence of at least three different components with S2p3/2 peak maxima at 161.5, 162.3, 163.7 and 168.1 eV, which are characteristic of S^{2-}, S_n^{2-}, S(0) and SO_4^{2-}, respectively [32–34]. The S2p signal from S-nZVI with S/Fe = 0.1 only shows the presence of trace amounts of sulfur in SO_4^{2-} form at the surface. The observation of these anionic species supports the presence of Fe(II) in these samples, which is presumably the origin of the observed new arbitrary peak in the Fe2p spectrum at the lower binding energy region. It is worth noting that the fraction of atomic concentrations of S species in S-nZVI samples with respect to the unknown Fe(II) component observed at 709 eV makes up ~10% at a S/Fe ratio of 0.1 and ~70% at a S/Fe ratio of 0.6. This observation suggests the presence of various Fe(II) compounds on the S-nZVI surface that have formed from sulfidation of the Fe(III) compounds, likely from the ferric oxide/oxyhydroxide layer [7]. In the same line, a mixture of Sn^{2-}, S^{2-} and SO_4^{2-} is typically found in the S-containing shells of sulfidized ZVI produced with Na_2S [5,14,35] and is explained as the result of a complex corrosion reaction between FeS and the Fe(0) core, including the formation of a ferric oxyhydroxide shell [4].

It should be noted that the doublet with a maximum observed at 163.7 eV from the S-nZVI particle with a S/Fe ratio of 0.6 should be interpreted with care due to the following reason: in XPS, the elemental sulfur shows a characteristic doublet with a maximum at 163.7 eV; on the other hand, polysulfides are chains with two different types of sulfur atoms; one at the end of the chains with a negative formal charge (terminal-S) and the other is a

non-terminal sulfur/s with no formal charge (central-S) [34]. On S-nZVI particle with S/Fe ratio of 0.6, the presence of polysulfides is evident from Figure 2b (green peaks), whereas the peak at 163.7 eV (violet peaks) could be originating from either elemental S or central-S from polysulfides or a combination of both. Based on the area under the peaks observed, the concentration of S^{2-}, S_n^{2-} (terminal-S) and S(0) (both elemental and central-S) on these particles is determined to be 36%, 18% and 46%, respectively.

The relative atomic concentration of Fe and S of these samples was determined based on the Fe2p and S2p peak area, collected in Table 2, which clearly demonstrates that with increasing S/Fe ratio, the overall S content increases on the S-nZVI surface. However, the ratio of the S content detected by the surface-sensitive XPS technique is much lower (S_{XPS}_0.6: S_{XPS}_0.1 = 4) than the ratio detected by the bulk analysis (TRIS extraction) method (S_{TRIS}_0.6: S_{TRIS}_0.1~16), suggesting a substantially higher S content at the surface compared to the bulk of the sample, with a S/Fe ratio of 0.1.

Table 2. Relative atomic concentration of Fe, S and Se components on S-nZVI surface, before and after their reaction with Se(VI) mixtures, determined from the respective XPS peak area.

Samples	Before Reaction		After Reaction		
	Fe (%)	S (%)	Fe (%)	S (%)	Se (%)
S/Fe = 0	100	0	95	0	5
S/Fe = 0.1	94	6	83	0	17
S/Fe = 0.6	76	24	70	10	20

Collectively, our observations demonstrate that exposure of nZVI to water for 48 h in the presence of dissolved oxygen led to the formation of a surface ferric oxyhydroxide layer. Sulfidation of nZVI generates a thin layer of S extractable as AVS, presumably FeS [15]. Upon exposure to water for 48 h, surface-bound Fe(II)-polysulfides FeS_x form in addition to FeS (Table 1), presumably associated with a ferric oxyhydroxide coating of the Fe(0) core. The shift in S fractionation from initially almost pure FeS to FeSx is indicative of an oxidation process, in which sulfide is oxidized to polysulfides. Similar observations were made during the sulfidation reaction of ferric oxyhydroxides, in which, after 2 h of reaction of lepidocrocite (γ-FeOOH) with sulfide, an FeS rim has formed around the lepidocrocite crystals [36], which collapsed after 2–3 days to generate surface-bound polysulfides [33].

3.2. Reaction of S-nZVI in the Presence of Se

The peak intensity of magnetite, a typical product of the reaction between Fe(0) and Se(IV) [37], increased with increasing Se(VI) loading, and it was the most dominant oxidation product formed in all experiments (Figure 1c,d). At the highest loading of Se(VI) (50 mg L^{-1}), the peak intensity of Fe(0) substantially decreased.

XPS analysis of the samples containing Fe, S and Se is complex as multiple emission signals of respective elements interfere with each other. For instance, S2p and Se3p (Figures 2 and S5), and Se3d and Fe3p [38] emission signals share the same spectral window. Thus, to resolve the discrete peaks, XPS of a series of Se compounds with 2−, 0, 4+ and 6+ oxidation state focusing on Se3d, Se3p and Se LMM (Auger signal from XPS measurement) regions were measured under similar experimental conditions, and are displayed in Figure S5 The correlative assessment of these reference signals helps to assign the chemical nature/formal oxidation state of the Se components observed on S-nZVI particles.

The measured S2p/Se3p, Se LMM and Fe2p spectra of S-nZVI samples treated with Se(VI) are shown in Figure 3 and Figure S6, respectively. In the Se LMM region, a broad signal with a maximum at ca. 179 eV and a weak shoulder at low binding energy was observed from all three samples. By comparing with similar profiles from the reference

samples (Figure S5), it was deduced that these are characteristic of Se with either "0" or "-II" oxidation state. This observation clearly evidences the effective reduction of Se(VI) by S-nZVI. Further, the exact oxidation state of the reduced Se products was identified by analyzing the detailed spectra in the S2p/Se3p region. In this region, two peaks were observed from S-nZVI samples with S/Fe concentration ratios of 0 and 0.1 with maxima at 161.8 eV and 167.2 eV and with an area intensity ratio of 0.35, which match the characteristics of Se3p3/2 and Se3p1/2 spin–orbit components from Se(0) (see Figure S5b). This observation is direct evidence for the reduction of Se(VI) to Se(0), the extent of which appears to increase with increasing sulfidation degree. Further, a similar assessment of signals from S-nZVI with S/Fe = 0.6 is complex, as S2p components interfere with Se3p signals in the same region. After careful consideration of signals observed from S-nZVI prior to Se(VI) reaction (see Figure 2b), the peak fitting was carried out, including the sulfur components. This results in three doublets with a Se3p3/2 maximum at 161.8 eV and two S2p3/2 maxima at 161.7 eV and 163.7 eV. Given the same peak maxima as above, the Se signal was assigned to Se(0) species, whereas the sulfur components should have originated from S^{2-} and S_n^{2-} species, as shown in Figure 2. Thus, all nZVI samples display reduction of Se(VI) to Se(0), and with increasing sulfur contents, appreciable amounts of sulfides and polysulfides were observed.

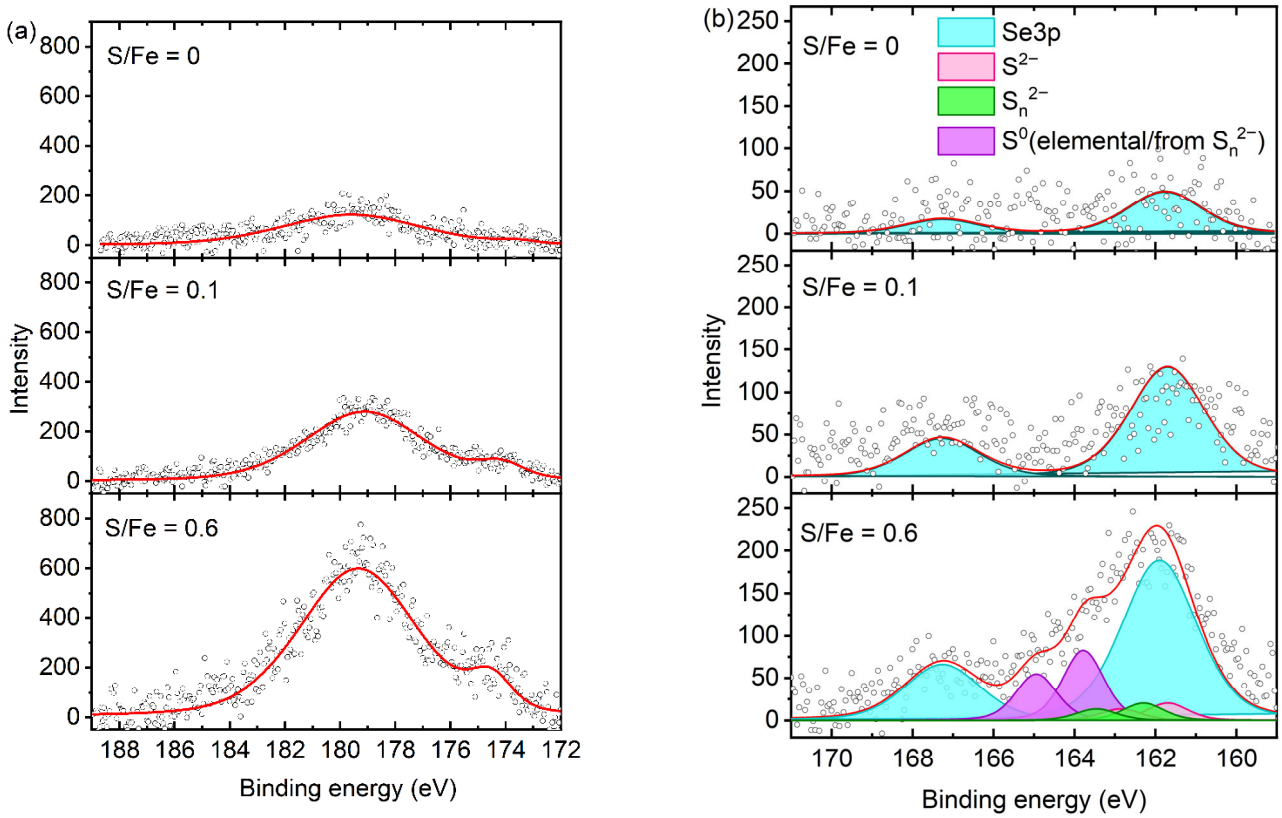

Figure 3. Detailed XPS of S-nZVI with S/Fe = 0, 0.1 and 0.6 concerning (**a**) Se LMM (Auger signal from XPS measurement) and (**b**) S2p regions after reacting with the Se(VI) (c = 50 mg L^{-1}).

The findings from XPS analysis are supported by XANES measurements demonstrating that Se(0) was the dominant product in all experiments. Between 79.5%–95.6% of the Se were recovered as Se(0) and 3.7%–19.4% as Se(IV) (Table S2, Figure S7). Similar fractions were determined both in unsulfidized [2] and sulfidized ZVI [7].

The Se3p/S2p region measured from S-nZVI with S/Fe = 0.1 (Figure 3b) exclusively shows Se3p peaks without any trace of sulfur components. Nevertheless, the same sample prior to reaction with Se(VI) displays trace amounts of sulfate species (Figure 2b), which

suggests either the sulfur species were consumed during the Se(VI) reduction reaction or the concentrations of the corresponding species are lower than the experimental limit. The latter assumption is supported by the low bulk AVS contents of this sample prior to the reaction (~5.5 mg g^{-1}, Table 1). Also, the relative intensity of the observed Fe(II) component from the same sample increased only slightly from 16% to 17.5% after reacting with Se(VI) (Figure S6). In contrast, on S-nZVI with a S/Fe ratio of 0.6, a clear effect of the reaction with Se(VI) is visible. The concentration of the S^{2-} content decreased from 36% to 17% after reacting with Se(VI) (Figures 2b and 3b), whereas the polysulfide (S_n^{2-}) concentration remains almost the same (18% to 17%), and the S^o concentration increased to 64% from 46%. Such a change in concentration of S compounds suggests the consumption of S^{2-} and consequent formation of either elemental sulfur or polysulfide chains, mostly central-S, during the reduction of Se(VI) into Se(0). Also, the low-binding-energy Fe(II) component (observed at 709.3 eV, Figure 2a) shows an increase in relative concentration after reaction with Se(VI) (Figure S6), indicating the formation of surface-bound Fe(II)-polysulfide species (FeS_x) [33]. Further quantitative analysis on Fe(II)/Fe(III) peaks was not pursued as it may mislead the discussion due to the significant interference of both Fe(II) and Fe(III) signals in this region [39].

These observations are underpinned by chemical extractions of reduced sulfur species after 48 h of reaction with Se(VI) (Table 1). The fraction of CRS comprises FeS2, surface-bound polysulfides (FeSx) and S(0) [40], while AVS extraction comprises only FeS, since polysulfides are regarded to be rather insensitive to acidic dissolution [41]. Sulfur concentrations recovered as TRIS were very similar for each S/Fe ratio (78 µmol g^{-1} +/− 15% at S/Fe-ratio = 0.1 and 1230 µmol g^{-1} +/− 8% S/Fe-ratio = 0.6), irrespective of the presence or absence of Se(VI).

In the absence of Se(VI), 48 h of reaction of the sulfidized layer led to the recovery of ~54% (S/Fe-ratio = 0.1) and ~65% (S/Fe-ratio = 0.6) of TRIS as CRS, indicating some shift in reduced sulfur speciation from FeS to S species with an oxidation state of zero. Since no evidence was found for the presence of pyrite (FeS_2), CRS presumably accounts mainly for surface-bound polysulfides FeS_x. At the low Se(VI) concentration, this value increased to ~68% and ~90%, respectively, and the fraction of CRS was even higher at the high Se(VI) concentration (~96% and ~91%). Hence, a substantial amount of polysulfide formation is connected to the presence of Se(VI), which is accompanied by the formation of Se(0).

3.3. Effect of Sulfidation on Se Removal

Removal of Se(VI) was observed in experiments with both nZVI and S-nZVI (Figure 4). A clear enhancement of the removal rate by sulfidation could be observed with almost 100% efficiency after 10 h at the low S/Fe ratio and at low Se concentration. Surprisingly, the rate decreased at the higher S/Fe ratio. The lowest rate and incomplete removal were observed without sulfidation. A similar dependence of the removal rate on the S/Fe ratio was observed in other studies for Cd^{2+}, Cr(VI), As(III) and Mo(VI) [5,6,42–46] and attributed to changes in surface properties of the iron sulfide shell with increasing S/Fe ratio, which reduced interactions with the contaminant [4,5].

The pattern was similar at the higher initial Se concentration, albeit the efficiency was lower in all three experimental settings at a concentration of 50 mg $L^{-1,}$ irrespective of the degree of sulfidation. Moreover, in order to fit the data properly, it was necessary to introduce a maximum of surface sites that are reactive (cf. SI, Section S3.5). As a consequence, the fraction of Se(VI) that was reduced with sulfidized nZVI is levelling off at similar values (~0.3).

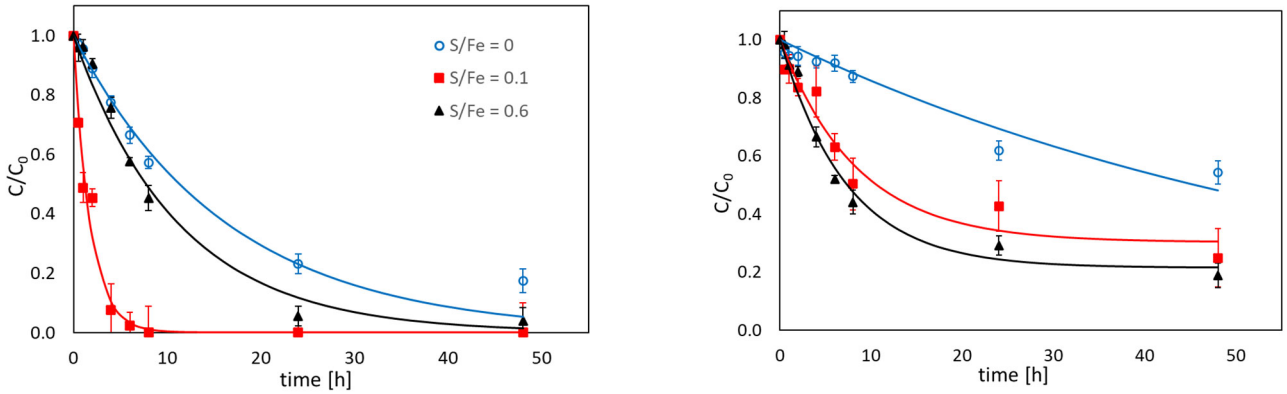

Figure 4. Se(VI) removal rates at different S/Fe ratios (0, 0.1 and 0.6): when (**a**) the Se(VI) concentration = 5 mg L^{-1} (63 µmol L^{-1}) and (**b**) when Se(VI) concentration = 50 mg L^{-1} (630 µmol L^{-1}). The solid lines are fitted from a 1st-order degradation model (cf. text for explanation). The error bars denote the ranges from measurements of duplicates.

Collectively, the results obtained from XPS analysis and the chemical extractions suggest involvement of surface species recovered as AVS in the reduction of Se(VI) and an internal conversion of the TRIS pool during the reaction. Hence, a stoichiometry can be formulated for the oxidation of the surface-bound FeS species >FeS to the surface-bound polysulfide species >FeS_x, with Se(0) being the main reduction product of Se(VI):

$$x\ {>}FeS + y/3\ SeO_4^{2-} + 8y/3\ H^+ \rightarrow FeS_x + y\ Fe^{2+} + y/3\ Se(0) + 4y/3\ H_2O \quad (1)$$

The factor x represents the number of S atoms and y (=x − 1) the number of elemental S(0) atoms bound in surface polysulfide so that the number of S(-II) atoms remains one.

Alternatively, XPS measurements also suggest the oxidation to surface-bound elemental sulfur (>S(0)):

$$>FeS + 1/3\ SeO_4^{2-} + 8/3\ H^+ = 1/3\ Se(0) + Fe^{2+} + >S(0) + 4/3\ H_2O \quad (2)$$

Equations (1) and (2) predict that the efficiency to reduce Se(VI) increases with increasing surface polysulfide length, which means that the number of >FeS surface sites required to reduce one SeO_4^{2-} ion decreases with increasing surface polysulfide length.

Both sulfidation and Se(VI) addition had substantial effects on pH (Figure 5). Samples containing n-ZVI particles generally had a pH of between 8.2 and 8.4. The addition of Se(VI) led to a slight acidification with an initial pH drop to 7.4 that recovered after 10 min. In contrast, sulfidized particles increased the pH to values between 9.5 and 10. Addition of Se(VI) to suspensions containing sulfidized particles led to a much stronger initial drop of pH, which reached a value of 3.2 at low sulfidation (S/Fe = 0.1) and which only slightly recovered until the end of the experiment. At a higher degree of sulfidation, the effect on pH was only observable for a Se(VI) concentration of 50 mg L^{-1}. The drop in pH was accompanied by a substantial release of Fe(II) in the presence of high concentrations of Se(VI) (Figure S8).

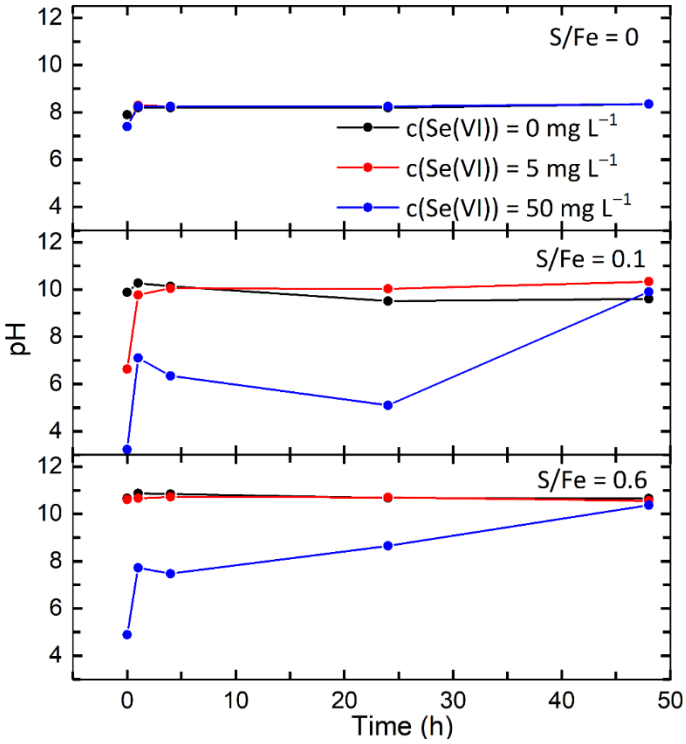

Figure 5. Change in pH during reaction of Se with nZVI and s-nZVI at different initial Se(VI) concentrations and S/Fe ratios.

The pH drop appears to be exclusively linked to the presence of Se(VI), which we relate to the oxidation of Fe(II) released upon reduction of Se(VI) by O_2 and the subsequent formation of a ferric oxyhydroxide, which we refer to as FeOOH in the following equation.

$$1.5\ H_2O + Fe^{2+} + ¼\ O_2 \rightarrow FeOOH + 2\ H^+ \quad (3)$$

The possible formation of FeOOH is also supported by the XPS analysis (Figure 2a). Note that formation of Fe^{2+} and its subsequent oxidation (and potential acidification) is common in reduction processes related to S-nZVI particles [7] and not specific to reactions (1) and (2), so that the individual contribution cannot be broken down. The net reaction of Equations (1) and (2) still predicts an alkaline reaction.

$$x\ FeS + y/3\ SeO_4^{2-} + 2y/3\ H^+ + y/6\ H_2O + y/4\ O_2 \rightarrow FeS_x + y\ FeOOH + y/3\ Se(0) \quad (4)$$

However, a kinetic decoupling between reaction (1) and (2) may be expected due to the very rapid oxidation of Fe(II) at the initially high pH values, which explains the initial pH drop and subsequent re-increase in the pH.

The stoichiometry from Equation (4) predicts that a large excess of >FeS species is required to completely consume even the low Se(VI) concentration and to become oxidized to FeS_x. Even at complete oxidation to elemental sulfur, approximately 190 µmol L^{-1} of the >FeS species would be required to oxidize the low Se(VI) concentration (5 mg L^{-1} = 63 µmol L^{-1}). However, at the low S/Fe ratio of 0.1, the initial amount of >FeS was only ~180 µmol L^{-1}. We therefore propose that two pathways were operating in parallel during the reduction of Se(IV): (i) a "classical" s-nZVI-based pathway in which the FeS shell channels electrons from the Fe(0) core to the contaminants [5,7], and (ii) a pathway in which surface-bound >FeS itself is involved.

In order to quantify the contribution of the surface-bound >FeS pathway to the overall degradation rate of Se(VI) by s-nZVI, we have quantified the consumption of AVS (as

measure for >FeS) in the presence of Se(VI) after 48 h (Table 1) and related it to the overall Se(VI) consumption rate after 48 h (Figure 4). The results from this estimate yield fractions of between 9 and 15% of the total degradation rate of Se(VI) (cf. Table S3 for the derivation of the fractions). Interestingly, the fraction appears to increase with increasing S/Fe ratio, which might point to a larger fraction of the surface-bound >FeS pathway contributing to the overall degradation rate under conditions, when the FeS layer becomes too thick and may inhibit the electron transfer rate [4].

4. Conclusions and Environmental Implications

Sulfidation of nZVI particles clearly increased the reduction rates of Se(VI). Here, we experimentally demonstrated the importance of reactive surface-bound reduced sulfur species formed upon sulfidation for the reduction process of Se(VI). Such involvement has been proposed [5,27], but has not been proven yet.

It can be assumed that these results can also be extrapolated to other oxyanions such as chromate [5]. Our findings thus have important implications for the effectiveness of the sulfidation processes for contaminant transformation. On the one hand, an increase in the yield of reactive sulfidation products may be desirable and shape the targeting design of S-nZVI. Zhang et al. [47] demonstrated the importance of the sulfur agents for FeSx formation and concluded that Na_2S or $Na_2S_2O_3$ led to the production of more FeS species compared to $Na_2S_2O_4$, where FeS_2 is a primary product. Moreover, sulfidation species forming upon reaction with naturally occurring ferric oxyhydroxides [48] may play a much more important role in the reduction of oxyanions [10] or oxycations [49] in the environment than previously assumed.

In this study, we were not able to fully elucidate the kinetic patterns observed in the experiments with higher rates of Se(VI) removal at the lower S/Fe ratio, and also a higher rate for lower Se(VI) concentrations. The difference may be due to a variation in pH with time, a difference in the formation of electron-conductive shells, but also in the occurrence of different pathways of Se(VI) reduction depending on the pool of reactive FeS species, as well as a pH-dependent change in the reactivity. More systematic studies in this direction are required that disentangle the intrinsic specific reactivity of the sulfidation products from the reactivity of ZVI obtained from stimulation through sulfidation.

Our observations may have direct implications for in situ treatment of, e.g., contaminated aquifers. Mass balance estimates demonstrate that the surface species >FeS substantially contributes to the overall degradation rate. Our data suggest that their relevance may even grow if the FeS layer thickness on the Fe(0) core (expressed by the molar S/Fe ratio) starts to have an inhibitory effect on the target reaction, i.e., the core-contaminant electron transfer. As a consequence, with increasing S/Fe ratio, S-nZVI particles may increasingly take on the properties of sulfidized ferric oxyhydroxides [48], which are regarded to be strongly involved in contaminant transformation [9]. This raises the question about the role such particles may play in contaminant remediation. As an alternative to the injection of S-nZVI particles, it may be better to inject sulfide into a (pretreated) ferric oxyhydroxide-rich aquifer to generate reactive surface sites.

Supplementary Materials: The following supporting information can be downloaded at: https://www.mdpi.com/article/10.3390/min16010068/s1. Table S1: measured S and Fe content in S-ZVI particles; Table S2: Fractions of different Se species in nZVI and S-nZVI derived from the LCF analysis of Se K-edge XANES; Table S3: Estimate of the fraction of Se(VI) reduced by surface bound >FeS; Table S4: Concentrations of Se (mean values) measured during removal experiments; Figure S1: TEM images provided by nZVI supplier NANOFER STAR; Figure S2: Quantitative phase analysis of XRD measurement of reference material nZVI provided by NANOFER STAR; Figure S3: SEM images of unreacted material; Figure S4: EDX spectra from nZVI and S-NZVI with different S/Fe

ratios; Figure S5: Detailed XPS of Se species; Figure S6: Detailed XPS of S-nZVI; Figure S7: Linear combination fitting with Se K reference XANES spectra of a sample containing 50 mg L^{-1} Se at a Fe/S ratio of 0.6; Figure S8: Fe(II) released from nZVI and S-nZVI after reaction with different Se(VI) concentrations; supporting methodological information can be found on the following: preparation of sulfidized nZVI particles, X-ray photo-electron spectroscopy, and X-ray absorption spectroscopy.

Author Contributions: Conceptualization, S.P. and B.M.; methodology, J.M., M.T. and J.G.; software, J.G. and K.H.; validation, J.M., M.T., K.H. and J.G.; formal analysis, S.P.; investigation, B.M.; resources, S.P.; data curation, S.P.; writing—original draft preparation, S.P., J.M. and B.M.; writing—review and editing, S.P.; visualization, J.M. and S.P.; supervision, S.P.; project administration, S.P.; funding acquisition, S.P. All authors have read and agreed to the published version of the manuscript.

Funding: This study was funded through the DFG grant PE 438/24-1.

Data Availability Statement: The original contributions presented in this study are included in the article/Supplementary Material. Further inquiries can be directed to the corresponding author(s).

Acknowledgments: We are grateful to Isolde Baumann for AVS and CRS analyses and extractions, and to Martina Heider for SEM/EDX measurements. We also acknowledge the XPS Facility (PHI 5000 VersaProbe III system) made available at the Keylab Device Engineering of Bavarian Polymer Institute (BPI) at the University of Bayreuth.

Conflicts of Interest: The authors declare no conflicts of interest.

References

1. Tang, C.; Huang, Y.H.; Zeng, H.; Zhang, Z. Reductive removal of selenate by zero-valent iron: The roles of aqueous Fe^{2+} and corrosion products, and selenate removal mechanisms. *Water Res.* **2014**, *67*, 166–174. [CrossRef] [PubMed]
2. Qin, H.; Li, J.; Yang, H.; Pan, B.; Zhang, W.; Guan, X. Coupled effect of ferrous ion and oxygen on the electron selectivity of zerovalent iron for selenate sequestration. *Environ. Sci. Technol.* **2017**, *51*, 5090–5097. [CrossRef] [PubMed]
3. Li, J.; Zhang, X.; Sun, Y.; Liang, L.; Pan, B.; Zhang, W.; Guan, X. Advances in sulfidation of zerovalent iron for water decontamination. *Environ. Sci. Technol.* **2017**, *51*, 13533–13544. [CrossRef] [PubMed]
4. Fan, D.; Lan, Y.; Tratnyek, P.G.; Johnson, R.L.; Filip, J.; O'Carroll, D.M.; Nunez Garcia, A.; Agrawal, A. Sulfidation of ironbased materials: A review of processes and implications for water treatment and remediation. *Environ. Sci. Technol.* **2017**, *51*, 13070–13085. [CrossRef]
5. Li, J.; Zhang, X.; Liu, M.; Pan, B.; Zhang, W.; Shi, Z.; Guan, X. Enhanced reactivity and electron selectivity of sulfidated zerovalent iron toward chromate under aerobic conditions. *Environ. Sci. Technol.* **2018**, *52*, 2988–2997. [CrossRef]
6. Li, H.; Zhang, J.; Gu, K.; Li, J. Sulfidation of zerovalent iron for improving the selectivity toward Cr(VI) in oxic water: Involvements of FeS_x. *J. Hazard. Mat.* **2020**, *409*, 124498. [CrossRef]
7. Fan, P.; Sun, Y.; Zhou, B.; Guan, X. Coupled effect of sulfidation and ferrous dosing on selenate removal by zerovalent iron under aerobic conditions. *Environ. Sci. Technol.* **2019**, *53*, 14577–14585. [CrossRef]
8. Gong, Y.; Gai, L.; Tang, J.; Fu, J.; Wang, Q.; Zeng, E.Y. Reduction of Cr(VI) in simulated groundwater by FeS-coated iron magnetic nanoparticles. *Sci. Total Environ.* **2017**, *595*, 743–751. [CrossRef]
9. Zhang, S.; Peiffer, S.; Liao, X.; Yang, Z.; Ma, X.; He, D. Sulfidation of ferric (hydr)oxides and its implication on contaminants transformation: A review. *Sci. Total Environ.* **2022**, *816*, 151574. [CrossRef]
10. Hockmann, K.; Planer-Friedrich, B.; Johnston, S.; Peiffer, S.; Burton, E. Antimony mobility in sulfidic systems: Coupling with sulfide-induced iron oxide transformations. *Geochim. Cosmochim. Acta* **2020**, *282*, 276–296. [CrossRef]
11. Zhou, J.; Chen, S.; Liu, J.; Frost, R.L. Adsorption kinetic and species variation of arsenic for As(V) removal by biologically mackinawite (FeS). *Chem. Eng. J.* **2018**, *354*, 237–244. [CrossRef]
12. Mullet, M.; Boursiquot, S.; Ehrhardt, J.-J. Removal of hexavalent chromium from solutions by mackinawite, tetragonal FeS. *Colloids Surf. A Physicochem. Eng. Asp.* **2004**, *244*, 77–85. [CrossRef]
13. Patterson, R.R.; Fendorf, S.; Fendorf, M. Reduction of Hexavalent Chromium by Amorphous Iron Sulfide. *Environ. Sci. Technol.* **1997**, *31*, 2039–2044. [CrossRef]
14. Han, D.S.; Batchelor, B.; Abdel-Wahab, A. Sorption of selenium(IV) and selenium(VI) to mackinawite (FeS): Effect of contact time, extent of removal, sorption envelopes. *J. Hazard. Mater.* **2011**, *186*, 451–457. [CrossRef] [PubMed]
15. Fordyce, F.M. Selenium Deficiency and Toxicity in the Environment. In *Essentials of Medical Geology*; Selinus, O., Ed.; Springer: Dordrecht, The Netherlands, 2013; pp. 375–416.

16. Paikaray, S.; Peiffer, S. Selenium enrichment, partitioning and leachability along semi-arid soils of NE Punjab, India. *Environ. Earth Sci.* **2024**, *83*, 272. [CrossRef]
17. Benis, K.Z.; McPhedran, K.N.; Soltan, J. Selenium removal from water using adsorbents: A critical review. *J. Hazard. Mater.* **2022**, *424*, 127603. [CrossRef]
18. Meher, A.K.; Jadhav, A.; Labhsetwar, N.; Bansiwal, A. Simultaneous removal of selenite and selenate from drinking water using mesoporous activated alumina. *Appl. Water Sci.* **2020**, *10*, 10. [CrossRef]
19. Yoon, I.H.; Kim, K.W.; Bang, S.; Kim, M.G. Reduction and adsorption mechanisms of selenate by zero-valent iron and related iron corrosion. *Appl. Catal B* **2011**, *104*, 185–192. [CrossRef]
20. Semerád, J.; Filip, J.; Ševců, A.; Brumovský, M.; Nguyen, N.H.A.; Mikšíček, J.; Lederer, T.; Filipová, A.; Boháčková, J.; Cajthaml, T. Environmental fate of sulfidated nZVI particles: The interplay of nanoparticle corrosion and toxicity during aging. *Environ. Sci. Nano* **2020**, *7*, 1794–1806. [CrossRef]
21. Tamura, H.; Goto, K.; Yotsuyanagi, T.; Nagayama, M. Spectrophotometric Determination of Iron(II) with 1,10-Phenanthroline in the Presence of large Amounts of Iron(III). *Talanta* **1974**, *21*, 314–318. [CrossRef]
22. Ravel, R.; Newville, M. ATHENA, ARTEMIS, HEPHAESTUS: Data analysis for X-ray absorption spectroscopy using IFEFFIT. *J. Synchrotron Radiat.* **2005**, *12*, 537–541. [CrossRef]
23. Canfield, D.E. Reactive iron in marine sediments. *Geochim. Cosmochim. Acta* **1989**, *53*, 619–632. [CrossRef] [PubMed]
24. Budd, M.S.; Bewick, H.A. Photometric determination of sulfide and reducible sulfur in alkalies. *Anal. Chem.* **1952**, *24*, 1536–1540. [CrossRef]
25. Brumovský, M.; Filip, J.; Malina, O.; Oborná, J.; Sracek, O.; Reichenauer, T.G.; Andrýsková, P.; Zbořil, R. Core–shell Fe/FeS nanoparticles with controlled shell thickness for enhanced trichloroethylene removal. *ACS Appl. Mater. Interfaces* **2020**, *12*, 35424–35434. [CrossRef] [PubMed]
26. Ribas, D.; Černík, M.; Benito, J.A.; Filip, J.; Marti, V. Activation process of air stable nanoscale zero-valent iron particles. *Chem. Eng. J.* **2017**, *320*, 290–299. [CrossRef]
27. Brumovský, M.; Oborná, J.; Lacina, P.; Hegedüs, M.; Sracek, O.; Kolařík, J.; Petr, M.; Kaslik, J.; Hofmann, T.; Filip, J. Sulfidated nano-scale zerovalent iron is able to effectively reduce in situ hexavalent chromium in a contaminated aquifer. *J. Hazard. Mater.* **2021**, *405*, 124665. [CrossRef]
28. Cornell, R.M.; Schwertmann, U. *The Iron Oxides: Structure, Properties, Reactions, Occurrences, and Uses*; Wiley-VCH: Weinheim, Germany, 2003.
29. Gupta, R.P.; Sen, S.K. Calculation of multiplet structure of core p-vacancy levels. II. *Phys. Rev. B* **1975**, *12*, 15. [CrossRef]
30. Biesinger, M.C.; Payne, B.P.; Grosvenor, A.P.; Lau, L.W.M.; Gerson, A.R.; Smart, R.S.C. Resolving surface chemical states in XPS analysis of first row transition metals, oxides and hydroxides: Cr, Mn, Fe, Co and Ni. *Appl. Surf. Sci.* **2011**, *257*, 2717–2730. [CrossRef]
31. Li, X.Q.; Zhang, W.X. Sequestration of metal cations with zerovalent iron nanoparticles a study with high resolution X-ray photoelectron spectroscopy (HR-XPS). *J. Phys. Chem. C* **2007**, *111*, 6939–6946. [CrossRef]
32. Pratt, A.R.; Muir, I.J.; Nesbitt, H.W. X-ray photoelectron and Auger electron spectroscopic studies of pyrrhotite and mechanism of air oxidation. *Geochim. Cosmochim. Acta* **1994**, *58*, 827–841. [CrossRef]
33. Wan, M.; Shchukarev, A.; Lohmayer, R.; Planer-Friedrich, B.; Peiffer, S. Occurrence of surface polysulphides during the interaction between ferric (hydr)oxides and aqueous sulphide. *Environ. Sci. Technol.* **2014**, *48*, 5076–5084. [CrossRef] [PubMed]
34. Fantauzzi, M.; Elsener, B.; Atzei, D.; Rigoldi, A.; Rossi, A. Exploiting XPS for the identification of sulfides and polysulfides. *RSC Adv.* **2015**, *5*, 75953–75963. [CrossRef]
35. Cao, Z.; Liu, X.; Xu, J.; Zhang, J.; Yang, Y.; Zhou, J.L.; Xu, X.; Lowry, G.V. Removal of antibiotic florfenicol by sulfide-modified nanoscale zero-valent iron. *Environ. Sci. Technol.* **2017**, *51*, 11269–11277. [CrossRef] [PubMed]
36. Hellige, K.; Pollok, K.; Larese-Casanova, P.; Behrends, T.; Peiffer, S. Pathways of ferrous iron mineral formation upon sulfidation of lepidocrocite surfaces. *Geochim. Cosmochim. Acta* **2012**, *81*, 69–81. [CrossRef]
37. Xia, X.; Ling, L.; Zhang, W.X. Solution and surface chemistry of the Se (IV)-Fe (0) reactions: Effect of initial solution pH. *Chemosphere* **2017**, *168*, 1597–1603. [CrossRef]
38. Shimada, K.; Mizokawa, T.; Mamiya, K.; Saitoh, T.; Fujimori, A.; Kamimura, T. Fe chalcogenides by X-ray photoemission spectroscopy. *Surf. Sci. Spectra* **1999**, *6*, 321–336. [CrossRef]
39. Gu, Y.; Wang, B.; He, F.; Bradley, M.J.; Tratnyek, P.G. Mechanochemically sulfidated microscale zero valent iron: Pathways, kinetics, mechanism, and efficiency of trichloroethylene dechlorination. *Environ. Sci. Technol.* **2017**, *1*, 12653. [CrossRef]
40. Peiffer, S.; Behrends, T.; Hellige, K.; Larese-Casanova, P.; Wan, M.; Pollok, K. Pyrite formation and mineral transformation pathways upon sulfidation of ferric hydroxides depend on mineral type and sulfide concentration. *Chem. Geol.* **2015**, *400*, 44–55. [CrossRef]
41. Rickard, D.; Morse, J.W. Acid volatile sulfide (AVS). *Mar. Chem.* **2005**, *97*, 141–197. [CrossRef]

42. Su, Y.; Adeleye, A.S.; Keller, A.A.; Huang, Y.; Dai, C.; Zhou, X.; Zhang, Y. Magnetic sulfide-modified nanoscale zerovalent iron (S-nZVI) for dissolved metal ion removal. *Water Res.* **2015**, *74*, 47–57. [CrossRef]
43. Wu, D.; Peng, S.; Yan, K.; Shao, B.; Feng, Y.; Zhang, Y. Enhanced As (III) sequestration using sulfide-modified nano-scale zero-valent iron with a characteristic core–shell structure: Sulfidation and as distribution. *ACS Sustain. Chem. Eng.* **2018**, *6*, 3039–3048. [CrossRef]
44. Shao, Q.; Xu, C.; Wang, Y.; Huang, S.; Zhang, B.; Huang, L.; Tratnyek, P.G. Dynamic interactions between sulfidated zerovalent iron and dissolved oxygen: Mechanistic insights for enhanced chromate removal. *Water Res.* **2018**, *135*, 322–330. [CrossRef]
45. Lv, D.; Zhou, J.; Cao, Z.; Xu, J.; Liu, Y.; Li, Y.; Yang, K.; Lou, Z.; Lou, L.; Xu, X. Mechanism and influence factors of chromium (VI) removal by sulfide-modified nanoscale zerovalent iron. *Chemosphere* **2019**, *224*, 306–315. [CrossRef]
46. Lian, J.J.; Yang, M.; Wang, H.L.; Zhong, Y.; Chen, B.; Huang, W.L.; Peng, P.A. Enhanced molybdenum (VI) removal using sulfide-modified nanoscale zerovalent iron: Kinetics and influencing factors. *Water Sci. Technol.* **2021**, *83*, 297–308. [CrossRef]
47. Zhang, Y.; Qiao, P.; Duan, Z.; Xu, C. Dominant pathways of FeSx formation and evolution during sulfidation of zero-valent iron by different sulfur agents. *Sep. Purif. Technol.* **2024**, *330*, 125280. [CrossRef]
48. Wan, M.; Schröder, C.; Peiffer, S. Fe(III):S(-II) Concentration Ratio Controls the Pathway and the Kinetics of Pyrite Formation during Sulfidation of Ferric Hydroxides. *Geochim. Cosmochim. Acta* **2017**, *217*, 334–348. [CrossRef]
49. Alexandratos, V.G.; Behrends, T.; van Cappellen, P. Sulfidization of lepidocrocite and its effect on uranium phase distribution and reduction. *Geochim. Cosmochim. Acta* **2014**, *142*, 570–586. [CrossRef]